

Reduced sensitivity to process, voltage and temperature variations in activated perpendicular magnetic tunnel junctions based stochastic devices

Md Golam Morshed,^{1, a)} Laura Rehm,² Ankit Shukla,³ Yunkun Xie,⁴ Samiran Ganguly,⁵ Shaloo Rakheja,³ Andrew D. Kent,² and Avik W. Ghosh^{1,6}

¹⁾ *Department of Electrical and Computer Engineering, University of Virginia, Charlottesville, VA 22904, USA*

²⁾ *Center for Quantum Phenomena, Department of Physics, New York University, New York, NY 10003, USA*

³⁾ *Department of Electrical and Computer Engineering, University of Illinois at Urbana-Champaign, Urbana, IL 61801, USA*

⁴⁾ *San Jose, CA, 95134, USA*

⁵⁾ *Department of Electrical and Computer Engineering, Virginia Commonwealth University, Richmond, VA 23284, USA*

⁶⁾ *Department of Physics, University of Virginia, Charlottesville, VA 22904, USA*

(Dated: 31 October 2023)

True random number generators (TRNGs) are fundamental building blocks for many applications, such as cryptography, Monte Carlo simulations, neuromorphic computing, and probabilistic computing. While perpendicular magnetic tunnel junctions (pMTJs) based on low-barrier magnets (LBMs) are natural sources of TRNGs, they tend to suffer from device-to-device variability, low speed, and temperature sensitivity. Instead, medium-barrier magnets (MBMs) operated with nanosecond pulses — denoted, stochastic magnetic actuated random transducer (SMART) devices — are potentially superior candidates for such applications. We present a systematic analysis of spin-torque-driven switching of MBM-based pMTJs ($E_b \sim 20 - 40 k_B T$) as a function of pulse duration (1 ps to 1 ms), by numerically solving their macrospin dynamics using a 1-D Fokker–Planck equation. We investigate the impact of voltage, temperature, and process variations (MTJ dimensions and material parameters) on the switching probability of the device. Our findings indicate SMART devices activated by short-duration pulses ($\lesssim 1$ ns) are much less sensitive to process-voltage-temperature (PVT) variations while consuming lower energy (\sim fJ) than the same devices operated with longer pulses. Our results show a path toward building fast, energy-efficient, and robust TRNG hardware units for solving optimization problems.

True random number generators (TRNGs) are employed in many applications, including cryptography,¹ Monte Carlo simulations,² neuromorphic computing,³ and probabilistic⁴ and stochastic computing.⁵ Conventional software algorithm-based and CMOS-based random number generators, e.g., linear-feedback shift registers do not serve the purpose of TRNG units because they produce pseudorandom bitstreams that are correlated and can be predetermined if the initial seed is known.^{6–8} In contrast, TRNGs utilize physical phenomena that are inherently random in nature, such as thermal noise, and radioactive decay.^{9–12} Existing CMOS-based implementations of TRNGs use thermal jitter for generating true random numbers; however, they have large footprints and are energy-hungry.^{13–15}

Spintronic TRNGs provide a new opportunity in this regard.^{16–18} Magnetic tunnel junctions (MTJs) constitute a fundamental building block for spintronic devices and are compatible with CMOS technology.^{19,20} MTJs consist of two ferromagnetic layers — a “pinned layer” whose magnetization is fixed and a “free layer” whose magnetization can be reoriented by a spin current — separated by an insulator. The relative orientation between the magnetization of the pinned layer and that of the free layer gives rise to parallel (P) and anti-parallel (AP)

states. The free layer of a MTJ exhibits a double potential well corresponding to two low energy states along the easy axis, separated by an energy barrier E_b . The magnetization state of the free layer can be switched from P to AP and vice versa by applying a current/voltage pulse, which utilizes spin-transfer torque (STT) to overcome the energy barrier.^{21–23} Such STT-driven MTJs show a prominent stochastic switching behavior in the presence of a thermal field^{24,25} that will form the basis of our analysis.

In the past, MTJs consisting of high-barrier magnets (HBMs, $E_b > 40 k_B T$, where k_B and T are the Boltzmann constant and temperature, respectively) were frequently advocated as TRNG units; however, they suffer from high energy costs and low throughput.^{16,26,27} At the opposite end of the spectrum, superparamagnetic tunnel junctions employing low-barrier magnets (LBMs, $E_b \sim k_B T$) have also been advocated as probabilistic bits. These LBMs allow the magnetization states to randomly fluctuate between P and AP, under the influence of the thermal field.^{28–30} Although the process is very energy-efficient, LBMs suffer from slow dynamics and are rather sensitive to process and temperature variations that degrade the quality of the random bitstreams. Besides, they require near-perfect circular cross sections, and are thus hard to build in practice.^{28,31,32} Stochastic magnetic actuated random transducer (SMART) devices based on perpendicular MTJs with medium-barrier magnets (MBMs, $E_b \sim 20 - 40 k_B T$) seem like a good com-

^{a)} Author to whom correspondence should be addressed: mm8by@virginia.edu

promise between these two extremes, for building energy-efficient and robust TRNG units.^{33,34} However, a systematic analysis of their energy-delay-reliability-variability trade-off has not yet been undertaken to our knowledge.

In this letter, we present a comprehensive analysis of STT-driven SMART TRNGs. We numerically solve the Fokker–Planck (FP) equation to calculate the 50% switching probability across a wide range of pulse durations (Fig. 1) and analyze the effect of different kinds of variations on this probability. Specifically, our study investigates the influence of pulse amplitude and duration (Fig. 2), temperature (Fig. 3), and geometric and material parameters (Fig. 4) on the 50% switching probability. We find that SMART devices exhibit relatively low sensitivity to the process-voltage-temperature (PVT) variations but a greater sensitivity to pulse duration variation, especially when operated under a short-pulse limit. We estimate the energy dissipated during stochastic switching (Fig. 5) and find that short pulse-activated switching consumes less energy than the same device operated with longer pulses, which suggests that SMART devices operating in the short-pulse limit can achieve robustness and energy efficiency concurrently. Our results provide a potential pathway toward the realization of fast, energy-efficient, and robust TRNG operations.

The dynamics of magnetization is commonly described by the stochastic macrospin Landau-Lifshitz-Gilbert (LLG) equation, given by:

$$\frac{1 + \alpha^2}{\gamma} \cdot \frac{\partial \mathbf{m}}{\partial t} = -\mu_0 \cdot (\mathbf{m} \times \mathbf{H}_{\text{eff}}) - \alpha \mu_0 \cdot \mathbf{m} \times (\mathbf{m} \times \mathbf{H}_{\text{eff}}) - \frac{\hbar}{2e} \cdot \frac{\eta I}{M_s \Omega} \cdot \mathbf{m} \times (\mathbf{m} \times \mathbf{m}_p), \quad (1)$$

where $\mathbf{m} = \mathbf{M}/M_s$ is the normalized magnetization and M_s is the saturation magnetization. I is the applied charge current and \mathbf{m}_p is the unit vector along the spin polarization direction. α , μ_0 , γ , η , \hbar , e , and Ω are the magnetic damping coefficient, permeability of free space, gyromagnetic ratio, spin polarization efficiency factor, reduced Planck constant, elementary charge, and volume of the MTJ free layer, respectively. In the absence of an external field, the effective field \mathbf{H}_{eff} includes the effective anisotropy field \mathbf{H}_k , and thermal field \mathbf{H}_{th} ($\mathbf{H}_{\text{eff}} = \mathbf{H}_k + \mathbf{H}_{\text{th}}$). The thermal field provides a random stochastic field, which can be incorporated in a Monte Carlo solution of the above differential equation.

Alternatively and more efficiently, by solving a Fokker-Planck (FP) equation, we can quantify the statistical nature of magnetization switching under thermal fluctuations.^{24,35–37} We numerically solve the 1-D differential equation form of the general FP equation:

$$\frac{\partial \rho}{\partial t} = -\nabla \cdot (\mathbf{L}\rho) + D_i \nabla^2 \rho,$$

where $\rho(\theta; t)$ is the probability density of the magnetization at time t , θ being the magnetization angle to the easy

axis (z -axis). \mathbf{L} is the sum of all the effective torques and D_i is the effective diffusive constant that accounts for the thermal fluctuations and is defined as:

$$D_i = \frac{\alpha \gamma k_B T}{(1 + \alpha^2) \mu_0 M_s \Omega}.$$

The details of the numerical methods can be found in Ref.³⁷.

The probability of switching can then be estimated from the probability density of magnetization as follows:

$$P_{\text{sw}} = \int_{\pi/2}^{\pi} \rho(\theta; t) d\theta = 1 - \int_0^{\pi/2} \rho(\theta; t) d\theta. \quad (2)$$

STT-driven magnetization switching under applied current or voltage pulses can generally be categorized into two limits — ballistic and diffusive. Ballistic switching refers to the magnetization dynamics under short-duration pulses, while longer-duration pulses dictate the diffusive limit. In the ballistic limit, the short pulse transfers spin-angular momentum to the free layer of the MTJ, and there is little effect of thermal fluctuation during the pulsing. The switching probability in the ballistic limit for a macrospin model can be expressed as:^{33,38}

$$P_{\text{sw}}^{\text{ballistic}} = \exp \left[-\frac{\pi^2 \Delta}{4} \exp \left\{ -\left(\frac{V}{V_{c0}} - 1 \right) \frac{2t_{\text{pw}}}{\tau_D} \right\} \right], \quad (3)$$

where thermal stability factor, $\Delta = E_b/k_B T = \mu_0 H_k M_s \Omega / 2k_B T$ and critical voltage for switching, $V_{c0} = 2\alpha e \mu_0 H_k M_s \Omega R_P / \eta \hbar$, R_P is the MTJ junction resistance in the P state. $\tau_D = (1 + \alpha^2) / \alpha \gamma \mu_0 H_k$ is the intrinsic time scale for the dynamics. $H_k = 2K_u / \mu_0 M_s - M_s$ is the anisotropy field, where K_u is uniaxial anisotropy constant. V and t_{pw} are the applied pulse amplitude and duration, respectively. In our simulations, we use an MBM having $\Delta \sim 35$ unless otherwise specified. The parameters used in the simulations are listed in Table I.

Figure 1(a) shows the probability density of an MBM ($\Delta \sim 35$) activated by a 1 ns pulse. The initial quasi-equilibrium Boltzmann distribution confined near the $\theta = 0$ well (θ is the angle between the magnetization and the z -axis) as shown by the blue curve in the top panel of Fig. 1(a). We turn ON the pulse at $t = 0$ ns. Immediately after pulsing at $t = 1.1$ ns, STT from the short duration pulse drives the probability density to the $\theta = \pi$ well, creating a bimodal distribution. If we relax the system for another nanosecond, we can clearly see the bimodal distribution leading to a 50% switching probability. The bottom panel of Fig. 1(a) shows the evolution of the probability density during the pulse duration. At the beginning of pulsing, the probability density is confined to the north pole of the unit Bloch sphere ($\theta = 0$) and starts spreading with time towards the south pole ($\theta = \pi$). Figure 1(b) shows a colorplot of the probability of switching P_{sw} as a function of pulse amplitude V , and pulse duration t_{pw} . As expected, the

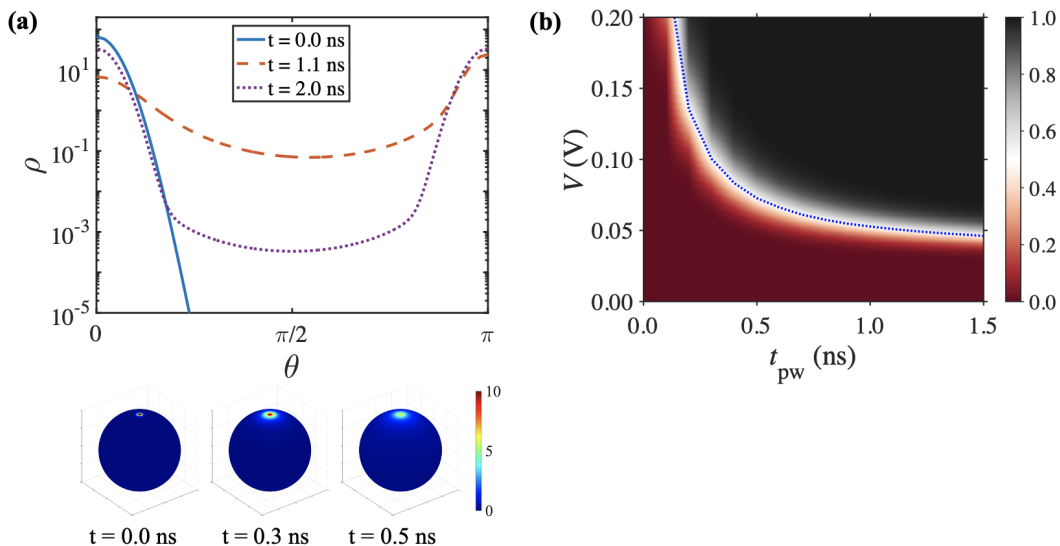


FIG. 1. (a) Probability density for an MBM ($\Delta \sim 35$) activated by a 1 ns pulse (top panel). The pulse is turned ON at $t = 0$ ns. A bimodal distribution emerges after the pulsing, which leads to a 50% switching probability. The bottom panel shows the time evolution of the probability density (colormap) during the pulsing. (b) Probability of switching (colormap) as a function of pulse amplitude and duration. The dotted blue overlaid curve represents a 50% switching probability.

pulse amplitude required for the magnetization switching is inversely proportional to the pulse duration.³⁹ The dotted blue overlaid curve shows the 50% switching probability, which is the ideal value of the TRNG operation. We aim to operate the device near this value.

The probability of switching can be tuned through pulse amplitude, V , and pulse duration, t_{pw} as shown in Fig. 1(b). For a specific pulse duration, we set the pulse amplitude (voltage) such that the probability of switching is 50%. We denote the voltage required for 50% switching probability as $V_{1/2}$. From Fig. 1(b), it is clear that $V_{1/2}$ will decrease as the t_{pw} increases and vice versa. However, both the $V_{1/2}$ and t_{pw} are subject to variation because, in reality, it is not feasible to apply an absolutely precise pulse amplitude and duration. We show the impact of such variations on the switching probability around the 50% midpoint (referred to as ‘midpoint switching probability’ hereafter) in Fig. 2. Figure 2(a) shows the change in midpoint switching probability as the pulse amplitude V is varied to be $\pm 10\%$ of $V_{1/2}$ for various pulse durations. We find the change of midpoint switching probability with respect to V , dP_{sw}/dV is lower for the short-pulse limit than for the longer pulse limit. On the other hand, Fig. 2(b) shows the change in midpoint switching probability to pulse duration t_{pw} for $\pm 10\%$ variations in t_{pw} . We get an opposite trend for the sensitivity to pulse duration. From Eq. (3), it can be shown that dP_{sw}/dV is proportional to pulse duration while dP_{sw}/dt_{pw} is proportional to $(V/V_{c0} - 1)$ around the $P_{sw} = 50\%$ value. Therefore, in the short-pulse limit, dP_{sw}/dV is lower while dP_{sw}/dt_{pw} is higher because short pulses require larger pulse amplitudes. Note that the pulse duration is kept fixed while we vary V . Similarly,

pulse amplitude remains fixed at the corresponding $V_{1/2}$ value during pulse duration variations. Also, note that for Fig. 2(b), we show data up to 20 ns because dP_{sw}/dt_{pw} becomes vanishingly small for longer pulses.

Temperature plays a critical role in STT-driven MTJ switching, as it directly impacts the functionality and reliability of the device.^{40,41} During the writing process, Joule heating can increase the junction temperature, which affects the device performance.⁴² The impact of thermal fluctuations mainly affects the initial magnetization distribution and the thermal stability factor ($\Delta = E_b/k_B T$). When the temperature increases from room temperature (300 K), the thermal stability factor decreases. Therefore, for a specific t_{pw} , with a fixed $V_{1/2}$, P_{sw} would be greater than 0.5. Similarly, P_{sw} would be less than 0.5 when temperature decreases below 300 K as it increases the thermal stability factor. As expected, Fig. 3(a) shows the linear relationship between the P_{sw} and T for a $\pm 10\%$ change in the temperature from room temperature. Figure 3(b) shows the dP_{sw}/dT for various pulse durations. We find that dP_{sw}/dT in the short-pulse limit is lower than for the longer-pulse limit. This higher sensitivity of dP_{sw}/dT in the diffusive limit arises from the double exponential dependence of P_{sw} on the energy barrier and temperature,

$$P_{sw}^{\text{diffusive}} = 1 - \exp\{-f_0 t_{pw} \exp(-E_b/k_B T)\}, \quad (4)$$

where f_0 is the attempt frequency. Interestingly, our FP-based result agrees well with the macrospin approximation in both ballistic and diffusive limits (Eqs. (3), (4)). Specifically, in the ballistic limit, dP_{sw}/dT can be estimated as $dP_{sw}^{\text{ballistic}}/dT = \ln 2/2T$ while for the diffusive limit, $dP_{sw}^{\text{diffusive}}/dT = (\ln 2/2T) \ln(f_0 t_{pw}/\ln 2)$ around

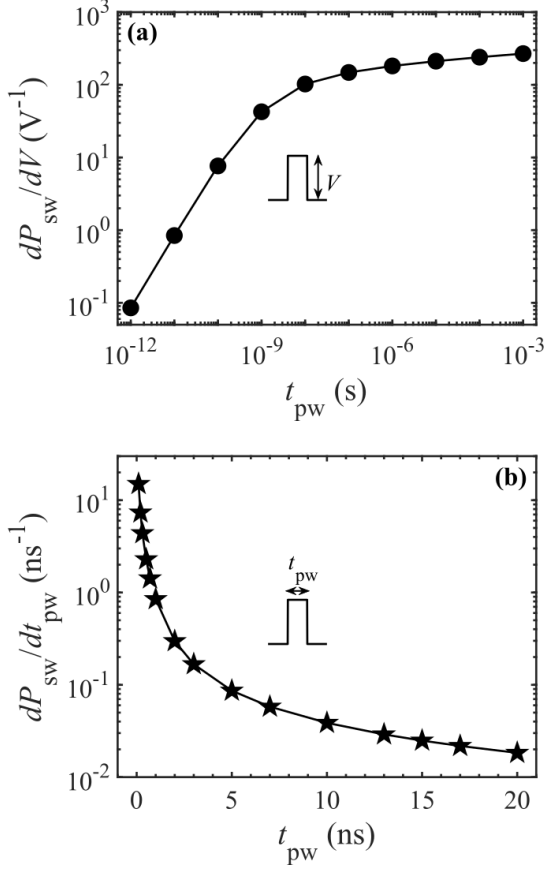


FIG. 2. Variation in midpoint switching probability with respect to (a) pulse amplitude and (b) pulse duration for various pulse durations.

the $P_{sw} = 50\%$ value. We use $f_0 = 1$ GHz, which is a commonly accepted value for magnetic materials.⁴³ We also show the dP_{sw}/dT for the MTJ free layer with lower and higher Δ values than that of MBM ($\Delta \sim 35$). We find that dP_{sw}/dT are similar regardless of the Δ values in the ballistic limit, while there is a slight variation in the dP_{sw}/dT in the diffusive limit, where a lower Δ value results in a higher temperature sensitivity.

We now move on to the impact of geometric and material parameter variation on the midpoint switching probability. Equation (3) suggests that for a specific pulse amplitude and duration, the probability of switching characteristic is driven by three quantities, namely Δ , V_{c0} , and τ_D . These quantities are all dependent on the geometric and material parameters of the free layer, and in practice are also susceptible to process variations during fabrication. It is thus critical to analyze the impact of parameter variation on the switching probability.⁴⁴

We show the impact of variation in free layer diameter D and thickness t_F and material parameters M_s , H_k , α , and η on the midpoint switching probability in Fig. 4. Among these parameters, D and t_F affect Δ and V_{c0} proportionally through volume, while α and H_k act like

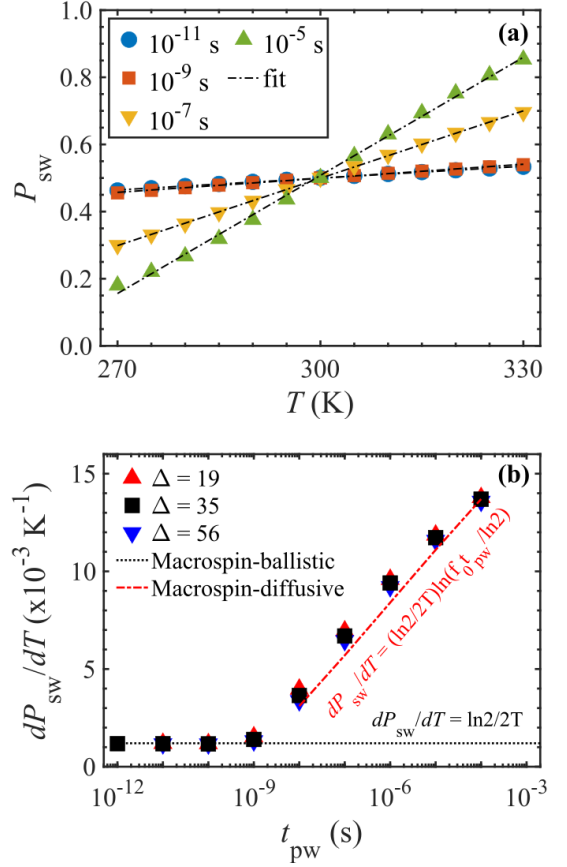


FIG. 3. (a) Variation in midpoint switching probability as a function of temperature for various pulse durations. The black dash-dotted lines show the linear fit. (b) Variation in midpoint switching probability with respect to temperature for a free layer with different thermal stability factors. The black and red dash-dotted lines in (b) represent the macrospin approximation in the ballistic (short pulse) and diffusive (long pulse) limits, respectively, and the texts represent the corresponding equation.

physical forces that oppose switching, affecting Δ and V_{c0} proportionally and τ_D inversely. For a fixed H_k , the parameter M_s has a similar effect on Δ and V_{c0} , while η only affects V_{c0} inversely. Overall, from Fig. 4, we find that for all kinds of parameter variations, the variation in the midpoint switching probability is weaker in the short-pulse limit than for longer pulses. This attribute indicates the robustness of the TRNG operation against process variations in short-pulse-activated SMART devices. While assessing parameter sensitivity, we keep $V_{1/2}$ fixed to its ideal value for a specific t_{pw} and vary only one parameter at a time. The percent variation for D , t_F , M_s , H_k , α , and η are $\pm 2.5\%$, $\pm 5\%$, $\pm 5\%$, $\pm 5\%$, $\pm 5\%$, $\pm 10\%$, respectively. We select these variations in ranges that each produce a linear fit with P_{sw} . Also, note that for H_k and α variations (Figs. 4(d) and 4(e)), we exclude very low pulse duration because at such small t_{pw} values, the interplay between Δ , V_{c0} , and τ_D changes P_{sw}

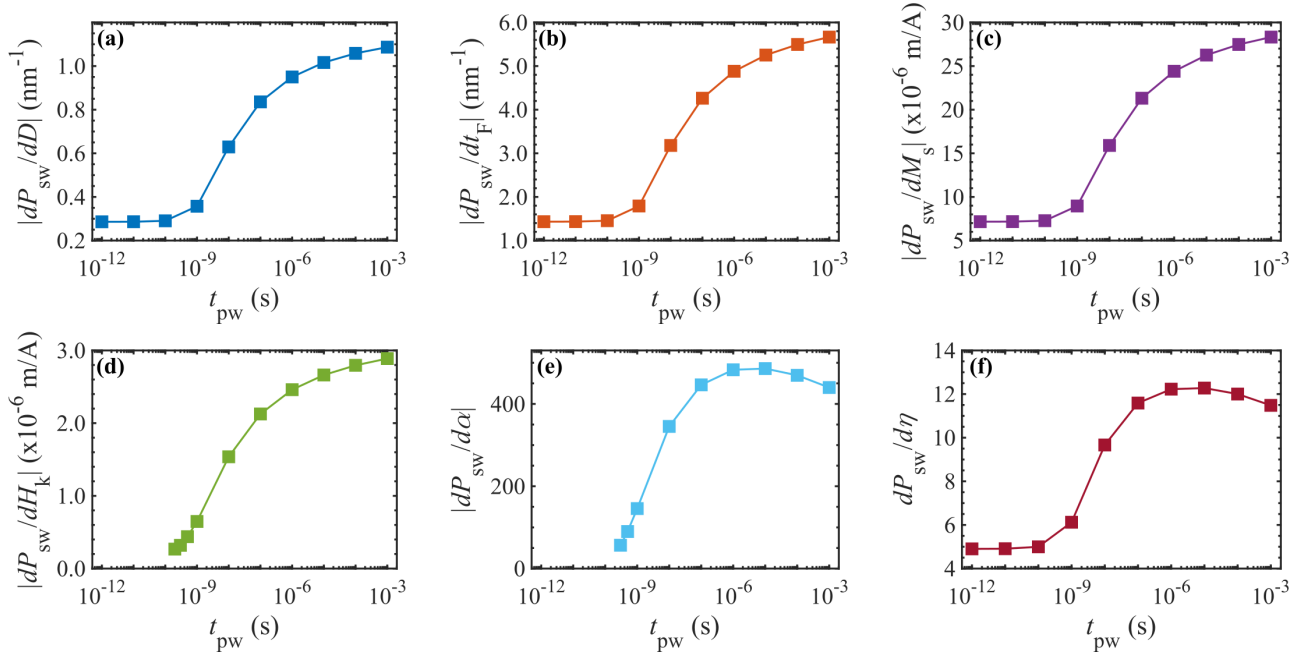


FIG. 4. Variation in midpoint switching probability with respect to (a) free layer diameter, (b) free layer thickness, (c) saturation magnetization, (d) anisotropy field, (e) magnetic damping coefficient, and (f) spin polarization efficiency factor for various pulse durations. For all the variations, the change in the midpoint switching probability is lower for the short pulse limit than the longer pulse limit, leading to robust TRNG operations.

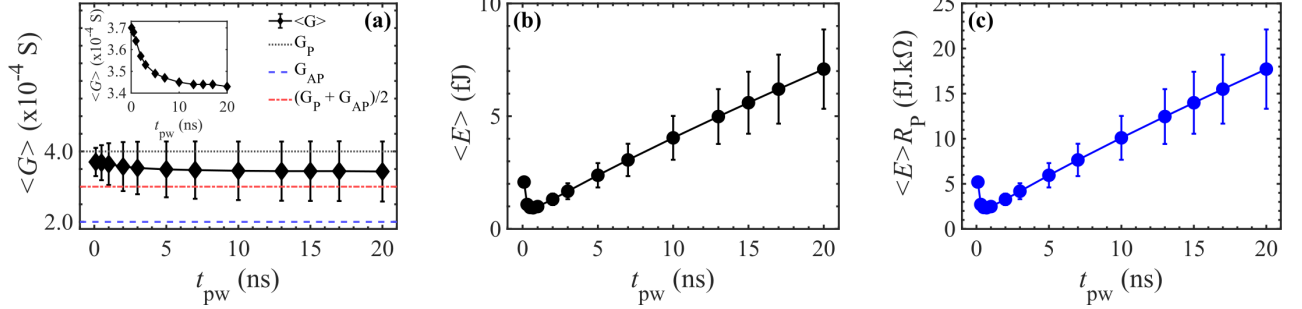


FIG. 5. (a) Average junction conductance, (b) average energy dissipation, and (c) average energy-resistance product for 50% switching for various pulse durations. In (a), the inset shows the zoomed view of $\langle G \rangle$. In all the figures, the error bars represent the standard deviation in our ensemble.

in such a way that we are unable to get a linear fit to the P_{sw} data with respect to H_k and α .

The above discussions on the 50% switching probability of the short-pulse driven MBM focus on robustness. However, the other important metric during switching is energy dissipation. Moreover, from Fig. 2, we can see that dP_{sw}/dV and dP_{sw}/dt_{pw} show opposite trends as a function of pulse duration. The energy dissipation metric can set the pulse limits for the device to achieve energy efficiency and robustness simultaneously. The STT-driven switching in the presence of a thermal field is stochastic and the junction conductance varies in time in a stochastic way. For a constant applied voltage, we can estimate the ensemble-averaged energy dissipation $\langle E \rangle = V^2 \langle G \rangle t_{pw}$, where $\langle G \rangle$ is the ensemble average of

the junction conductance during the pulse duration. One might assume $\langle G \rangle = (G_P + G_{AP})/2$, considering half the time the magnetization is in the P state, while in the other half, it is in the AP state (G_P and G_{AP} are the junction conductance in the P and AP state, respectively); however, it is not guaranteed that the magnetization will spend equal time in P and AP states. An accurate way is to employ the probability density obtained by solving the FP equation, $\langle G \rangle = \frac{1}{t_{pw}} \int_0^{t_{pw}} dt \int_0^\pi d\theta \rho(\theta; t) G(\theta)$, where $G(\theta) = \frac{1}{2}(G_P + G_{AP}) + \frac{1}{2}(G_P - G_{AP}) \cos \theta$.

Figure 5(a) shows the ensemble-averaged conductance $\langle G \rangle$ for various pulse durations. For short pulse duration, $\langle G \rangle$ is close to the G_P value, and as the pulse duration increases, $\langle G \rangle$ value decreases because the magnetization

TABLE I. Material parameters for MTJ free layer.

Symbol	Definition	Value
D (nm)	Diameter	15
t_F (nm)	Thickness	1.5
M_s (kA/m)	Saturation magnetization	300 ⁴⁷
K_u (kJ/m ³)	Uniaxial anisotropy	600 ⁴⁷
α	Damping coefficient	0.01 ⁴⁷
TMR	Tunnel magnetoresistance	100% ⁴⁸
R_P (R_{AP}) (k Ω)	Resistance in P (AP) state	2.5 (5.0)
η	Spin polarization efficiency	0.433

spends more time in the AP states (see inset for zoomed view). However, $\langle G \rangle$ starts to saturate for longer pulses. We conjecture that for longer pulses, the thermal energy started taking over, which limits the evolution of probability density to the AP states regardless of the pulse duration. If we consider $\langle G \rangle = (1 - k)G_P + kG_{AP}$, k varies from $\sim 15 - 30\%$ as a function of pulse duration. It is noteworthy that $\langle G \rangle$ is greater than $(G_P + G_{AP})/2$ throughout the range of the pulse duration. From $\langle G \rangle$ we calculate the ensemble averaged energy dissipation $\langle E \rangle$ in Fig. 5(b). We find a lower energy dissipation for the short-pulse limit over the longer-pulse limit. In the short-pulse limit, the energy dissipation is in the range of only a few femtojoules, which is orders of magnitude lower than the CMOS-based TRNG units (usually in the picojoules range).^{45,46} It should be noted, that we are only considering the random bit write (activation) energy here. Finally, we quote $\langle E \rangle R_P$ (in fJ.k Ω unit) because it is relatively easy to vary the R_P in the experiment ($R_P = 1/G_P$ is the junction resistance in the P state). Using the tunnel magnetoresistance (TMR) relation, $TMR = (G_P - G_{AP})/G_{AP}$ in the $G(\theta)$ equation, from straightforward algebra, it can be shown that the quantity $\langle E \rangle R_P$ depends only on the applied voltage, TMR, and the probability density obtained from the FP equation. In the short-pulse limit, for 100% TMR, $\langle E \rangle R_P$ is ~ 5 fJ.k Ω or lower. Note that in Fig. 5, we show data up to 20 ns because the energy dissipation is very high for longer pulses and is unsuitable for comparison with the short-pulse limit.

In summary, we demonstrate the suitability of MBM-based SMART devices for TRNG operations for a wide range of pulse durations. We studied the impact of various kinds of variations around the 50% percent switching probability. Furthermore, we evaluate the energy consumption associated with the stochastic switching process. Our results show that the SMART devices operating in the short-pulse limit ($\lesssim 1$ ns) can achieve both robustness and energy efficiency. Our findings offer insights into the development of fast, energy-efficient, and reliable TRNG units for various applications.

ACKNOWLEDGMENTS

This work was supported in part by the NSF I/UCRC on Multi-functional Integrated System Technology (MIST) Center; IIP-1439644, IIP-1439680, IIP-1738752, IIP-1939009, IIP-1939050, and IIP-1939012. The research at NYU was supported by the DOE Office of Science (ASCR/BES) Microelectronics Co-Design project COINFLIPS and by the Office of Naval Research (ONR) under award number N00014-23-1-2771. The authors at UIUC acknowledge the support of NSF through Award # CCF-1930620 and Air Force Research Laboratory under Grant # FA8750-21-1-0002. The calculations were performed using the computational resources from High-Performance Computing systems at the University of Virginia (Rivanna).

DATA AVAILABILITY

The data that support the findings of this study are available from the corresponding author upon reasonable request.

REFERENCES

- B. Sunar, in *Cryptographic Engineering* (Springer, Boston, MA, Boston, MA, USA, 2009) pp. 55–73.
- H. Bauke and S. Mertens, *Phys. Rev. E* **75**, 066701 (2007).
- S. Misra, L. C. Bland, S. G. Cardwell, J. A. C. Incorvia, C. D. James, A. D. Kent, C. D. Schuman, J. D. Smith, and J. B. Aimone, *Adv. Mater.* **35**, 2204569 (2023).
- K. Y. Camsari, R. Faria, B. M. Sutton, and S. Datta, *Phys. Rev. X* **7**, 031014 (2017).
- M. W. Daniels, A. Madhavan, P. Talatchian, A. Mizrahi, and M. D. Stiles, *Phys. Rev. Appl.* **13**, 034016 (2020).
- R. M. D'Souza, Y. Bar-Yam, and M. Kardar, *Phys. Rev. E* **57**, 5044 (1998).
- J. F. Fernández and C. Criado, *Phys. Rev. E* **60**, 3361 (1999).
- A. Poorghanad, A. Sadr, and A. Kashanipour, in *2008 International Conference on Computational Intelligence and Security* (IEEE) pp. 13–17.
- C. S. Petrie and J. A. Connelly, *IEEE Trans. Circuits Syst. I* **47**, 615 (2000).
- R. Brederlow, R. Prakash, C. Paulus, and R. Thewes, in *2006 IEEE International Solid State Circuits Conference - Digest of Technical Papers* (IEEE) pp. 06–09.
- A. Alkassar, T. Nicolay, and M. Rohe, in *Computational Science and Its Applications - ICCSA 2005* (Springer, Berlin, Germany, 2005) pp. 634–646.
- D. Ruschen, M. Schrey, J. Freese, and I. Heisterklaus, power **3**, 3V (2017).
- N. Liu, N. Pinckney, S. Hanson, D. Sylvester, and D. Blaauw, in *2011 Symposium on VLSI Circuits - Digest of Technical Papers* (IEEE) pp. 15–17.
- S. K. Mathew, S. Srinivasan, M. A. Anders, H. Kaul, S. K. Hsu, F. Sheikh, A. Agarwal, S. Satpathy, and R. K. Krishnamurthy, *IEEE J. Solid-State Circuits* **47**, 2807 (2012).
- S. K. Mathew, D. Johnston, S. Satpathy, V. Suresh, P. Newman, M. A. Anders, H. Kaul, A. Agarwal, S. K. Hsu, G. Chen, and R. K. Krishnamurthy, *IEEE J. Solid-State Circuits* **51**, 1695 (2016).
- A. Fukushima, T. Seki, K. Yakushiji, H. Kubota, H. Imamura, S. Yuasa, and K. Ando, *Appl. Phys. Express* **7**, 083001 (2014).
- A. Fukushima, T. Yamamoto, T. Nozaki, K. Yakushiji, H. Kubota, and S. Yuasa, *APL Mater.* **9** (2021), 10.1063/5.0038974.

- ¹⁸Z. Fu, Y. Tang, X. Zhao, K. Lu, Y. Dong, A. Shukla, Z. Zhu, and Y. Yang, *Front. Phys.* **9**, 638207 (2021).
- ¹⁹S. Matsunaga, J. Hayakawa, S. Ikeda, K. Miura, T. Endoh, H. Ohno, and T. Hanyu, in *2009 Design, Automation & Test in Europe Conference & Exhibition* (IEEE) pp. 20–24.
- ²⁰P. Barla, V. K. Joshi, and S. Bhat, *IEEE Access* **8**, 6876 (2020).
- ²¹J. Z. Sun, *Phys. Rev. B* **62**, 570 (2000).
- ²²Z. Diao, Z. Li, S. Wang, Y. Ding, A. Panchula, E. Chen, L.-C. Wang, and Y. Huai, *J. Phys.: Condens. Matter* **19**, 165209 (2007).
- ²³D. Bedau, H. Liu, J.-J. Bouzaglou, A. D. Kent, J. Z. Sun, J. A. Katine, E. E. Fullerton, and S. Mangin, *Appl. Phys. Lett.* **96** (2010), 10.1063/1.3284515.
- ²⁴W. F. Brown, *Phys. Rev.* **130**, 1677 (1963).
- ²⁵A. F. Vincent, J. Larroque, N. Locatelli, N. B. Romdhane, O. Bichler, C. Gamrat, W. S. Zhao, J.-O. Klein, S. Galdin-Retailleau, and D. Querlioz, *IEEE Trans. Biomed. Circuits Syst.* **9**, 166 (2015).
- ²⁶N. Rangarajan, A. Parthasarathy, and S. Rakheja, *J. Appl. Phys.* **121** (2017), 10.1063/1.4985702.
- ²⁷Y. Qu, B. F. Cockburn, Z. Huang, H. Cai, Y. Zhang, W. Zhao, and J. Han, *IEEE Trans. Nanotechnol.* **17**, 1270 (2018).
- ²⁸D. Vodenicarevic, N. Locatelli, A. Mizrahi, J. S. Friedman, A. F. Vincent, M. Romera, A. Fukushima, K. Yakushiji, H. Kubota, S. Yuasa, S. Tiwari, J. Grollier, and D. Querlioz, *Phys. Rev. Appl.* **8**, 054045 (2017).
- ²⁹D. Vodenicarevic, N. Locatelli, A. Mizrahi, T. Hirtzlin, J. S. Friedman, J. Grollier, and D. Querlioz, in *2018 IEEE International Symposium on Circuits and Systems (ISCAS)* (IEEE) pp. 27–30.
- ³⁰L. Schnitzspan, M. Kläui, and G. Jakob, *Phys. Rev. Appl.* **20**, 024002 (2023).
- ³¹Md. A. Abeed and S. Bandyopadhyay, *IEEE Magn. Lett.* **10**, ArticleSequenceNumber:4504405 (2019).
- ³²M. G. Morshed, S. Ganguly, and A. W. Ghosh, *IEEE Magn. Lett.* **14**, ArticleSequenceNumber:6100405 (2023).
- ³³L. Rehm, C. C. M. Capriata, S. Misra, J. D. Smith, M. Pinarbasi, B. G. Malm, and A. D. Kent, *Phys. Rev. Appl.* **19**, 024035 (2023).
- ³⁴A. Shukla, L. Heller, M. G. Morshed, L. Rehm, A. W. Ghosh, A. D. Kent, and S. Rakheja, in *2023 24th International Symposium on Quality Electronic Design (ISQED)* (IEEE) pp. 05–07.
- ³⁵W. H. Butler, T. Mewes, C. K. A. Mewes, P. B. Visscher, W. H. Rippard, S. E. Russek, and R. Heindl, *IEEE Trans. Magn.* **48**, 4684 (2012).
- ³⁶H. Liu, D. Bedau, J. Z. Sun, S. Mangin, E. E. Fullerton, J. A. Katine, and A. D. Kent, *J. Magn. Magn. Mater.* **358-359**, 233 (2014).
- ³⁷Y. Xie, B. Behin-Aein, and A. W. Ghosh, *IEEE Trans. Electron Devices* **64**, 319 (2016).
- ³⁸J. Z. Sun, *IBM J. Res. Dev.* **50**, 81 (2006).
- ³⁹D. Bedau, H. Liu, J.-J. Bouzaglou, A. D. Kent, J. Z. Sun, J. A. Katine, E. E. Fullerton, and S. Mangin, *Appl. Phys. Lett.* **96** (2010), 10.1063/1.3284515.
- ⁴⁰J. Cao, Y. Liu, Y. Ren, F. Wei, and P. P. Freitas, *Appl. Surf. Sci.* **314**, 443 (2014).
- ⁴¹B. Teso, S. Kravenkit, K. Sorn-in, A. Kaewrawang, A. Krue-subthaworn, A. Siritaratiwat, T. Mewes, C. K. A. Mewes, and C. Surawanitkun, *Appl. Surf. Sci.* **472**, 36 (2019).
- ⁴²D. H. Lee and S. H. Lim, *Appl. Phys. Lett.* **92** (2008), 10.1063/1.2943151.
- ⁴³L. Lopez-Diaz, L. Torres, and E. Moro, *Phys. Rev. B* **65**, 224406 (2002).
- ⁴⁴J. Song, H. Dixit, B. Behin-Aein, C. H. Kim, and W. Taylor, *IEEE Trans. Magn.* **56**, ArticleSequenceNumber:3400411 (2020).
- ⁴⁵S. K. Mathew, S. Srinivasan, M. A. Anders, H. Kaul, S. K. Hsu, F. Sheikh, A. Agarwal, S. Satpathy, and R. K. Krishnamurthy, *IEEE J. Solid-State Circuits* **47**, 2807 (2012).
- ⁴⁶K. Yang, D. Fick, M. B. Henry, Y. Lee, D. Blaauw, and D. Sylvester, in *2014 IEEE International Solid-State Circuits Conference Digest of Technical Papers (ISSCC)* (IEEE) pp. 09–13.
- ⁴⁷N. Kani, S. Rakheja, and A. Naemi, *IEEE Trans. Electron Devices* **63**, 4119 (2016).
- ⁴⁸S. Ota, M. Ono, H. Matsumoto, A. Ando, T. Sekitani, R. Kohno, S. Iguchi, T. Koyama, and D. Chiba, *Appl. Phys. Express* **12**, 053001 (2019).